Evaluation of a Perineal Access Device for MRI-Guided Prostate Interventions

Pezhman Foroughi[a], Purnima Rajan[a], Martin Hoßbach[a], Alican Demir[a], Jan Hämmelmann[a], Kenny Harlan[a], Aliza Mushtaq[b], Lance A. Mynderse[b], and David A. Woodrum[b]

[a]Clear Guide Medical, Baltimore, Maryland, USA
[b]Mayo Clinic, Rochester, Minnesota, USA

ABSTRACT

This paper describes a perineal access tool for MRI-guided prostate interventions and evaluates it using a phantom study. The development of this device has been driven by the clinical need and a close collaboration effort. The device seamlessly fits into the workflow of MRI-guided prostate procedures such as cryoablation and biopsies. It promises a significant cut in the procedure time, accurate needle placement, lower number of insertions, and a potential for better patient outcomes. The current embodiment includes a frame which is placed next to the perineum and incorporates both visual and MRI-visible markers. These markers are automatically detected both in MRI and by a pair of stereo cameras (optical head) allowing for automatic optical registration. The optical head illuminates the procedure area and can track instruments and ultrasound probes. The frame has a window to access the perineum. Multiple swappable grids may be placed in this window depending on the application. It is also possible to entirely remove the grid for freehand procedures. All the components are designed to be used inside the MRI suite. To test this system, we built a custom phantom with MRI visible targets and planned 21 needle insertions with three grid types using the SCENERGY software. With an average insertion depth of about 85 mm, the average error of needle tip placement was 2.74 mm. We estimated the error by manually segmenting the needle tip in post-insertion MRIs of the phantom and comparing that to the plan.

Keywords: Prostate Cancer, MRI-Guided, Navigation, MRI Intervention, Template grid, Biopsy, Ablation, Needle placement

1. INTRODUCTION

Over one million prostate biopsies are performed in the United States annually. Prostate cancer is the most prevalent solid organ cancer in males with more than a quarter of a million new cases per year and the second-leading cause of cancer deaths in men.[1] Most of prostate biopsies in the United States are performed with non-targeted systematic transrectal ultrasound (TRUS)-guided biopsy in patients with an elevated prostate serum antigen level and/or abnormal digital rectal examination. Non-targeted TRUS-guided biopsy typically obtains 12-core biopsy, which yields a considerably high false negative rate of cancer detection.[2,3] Furthermore, certain areas of the prostate gland (e.g., the anterior gland, transition zone and apex) are known to be under-sampled or not sampled at all at routine non-targeted TRUS-guided biopsy and are now increasingly being recognized as areas that may contain clinically significant tumors.[4]

TRUS biopsy has been the mainstay of prostate biopsy in the United States because it has a short learning curve, can be performed quickly using a simple rectal probe, and is performed under local anesthesia. However, chance of infection following transrectal (TR) prostate biopsy is relatively high ranging from 0.1% to 7.0% resulting in a high chance of sepsis ranging from 0.3% to 3.1%.[5] This risk is increasing because antibiotic-resistant bacteria are becoming more common.[6,7] The cost of treating sepsis is high approaching of hundreds of millions per year in the United States and still increasing.[7,8]

Internationally, the practice of using the transperineal approach (TP) has been growing. Increasing concerns about drug-resistant bacteria and repeat hospitalizations have shifted attention to that access route. Recent

Further author information: (Send correspondence to Pezhman Foroughi)
Pezhman Foroughi: E-mail: foroughi@clearguidemedical.com

articles show that various non-general anesthesia methods are able to effectively relieve the pain of the TP procedure,[4,9] and Bhatt et al.[10] showed that patients who had undergone both TR and TP preferred TP over TR 42% to 31%. A 2019 review[11] concluded that while TP biopsy offers the same diagnosis accuracy of TR prostate biopsy, the risk of infection and rectal bleeding is significantly lower making it a much safer alternative. The recommendation was to perform TP biopsy whenever possible in spite of a higher risk of pain. In January 2021, the European Association of Urology stated, "Available evidence highlights that it is time for the urological community to switch from a transrectal to a transperineal [prostate biopsy] approach despite any possible logistical challenges".[12]

TP prostate procedures often use a grid and TRUS for needle placement. Although TRUS is widely available and easy-to-use, MRI provides superior soft-tissue contrast, high spatial resolution, direct multiplanar imaging capabilities, and a large field of view. It is proven to be a valuable tool to visualize the prostate, diagnose, and stage prostate cancer.[13–15] Clinical systems such as UroNav (Philips, Amsterdam, Netherlands), ARTEMIS (innoMedicus, Cham, Switzerland), and KOELIS Trinity (KOELIS, Grenoble, France) can register pre-biopsy images with TRUS. However, image registration quality, glandular deformation, needle tracking and operator experience may impact accuracy for these systems. As a result these systems may not offer an advantage compared to TP biopsy with cognitive fusion.[16] In-bore MRI-guided TP biopsy can eliminate the need for this registration. However, long MRI scanner time required for the procedure and the limited availability of guidance solutions has prevented its wide adoption.

Significant research and development have been devoted toward robotic solutions for MR-guided TP procedures (biopsies, ablations or brachytherapies).[17–19] Proposed solutions either employ MR-safe pneumatic actuators, which fully block the bore and require additional infrastructure with tubing connections in the Zone 4 for compressed air, or incorporate ultrasonic /piezoelectric motors, which are still emerging. Indeed, to our knowledge, only one MR-compatible robotic solution is reported to gain FDA approval.[20] While robotic technologies with integrated guidance are very promising in terms of accuracy and repeatability, clinical research performed in patients remains limited and thus clinical value is yet to be firmly established.[21,22]

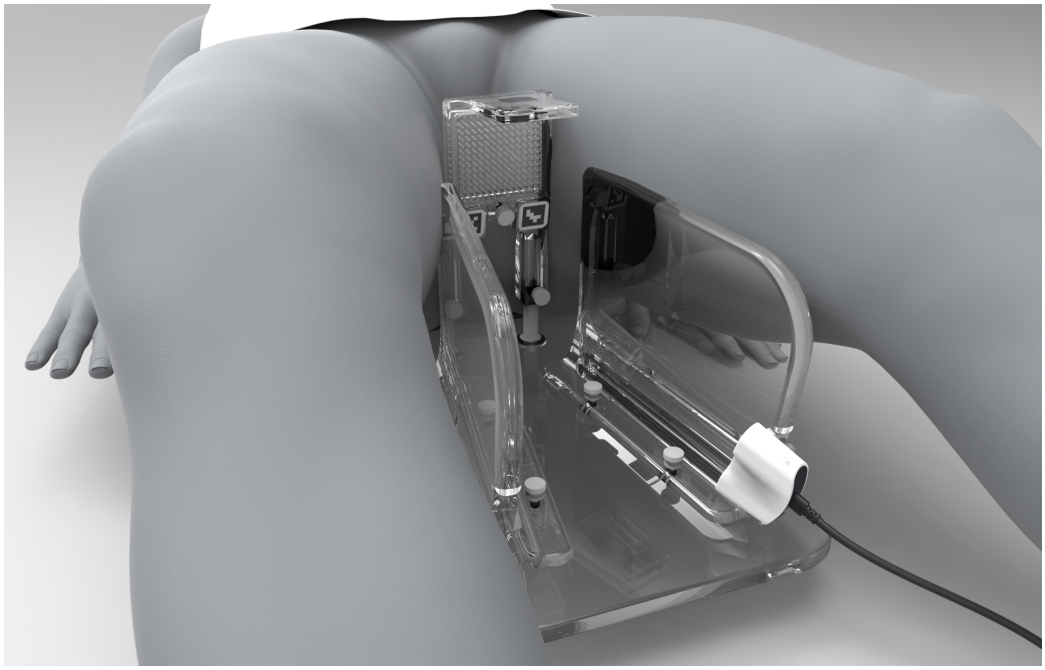

Figure 1. Clear Guide customized prostate guidance device.

Here, we introduce a solution which potentially simplifies the current workflow, improves targeting accuracy, and reduces the number of repetitive MRI scan sequences needed to verify needle placement. As a result, it significantly reduces the procedure time. The hope is for this system to enable more physicians to feel comfortable

with the TP approach with MRI-guidance. It is comprised of a hardware piece shown in Figure 1, and a software program. The hardware is designed to be used inside the MR room and provides a window for perineal access. The clinician is still in charge and performs the planning on the software and inserts the needle following the guidance. The access window can accommodate a grid or can be left open for freehand needle placement.

This system has a small footprint with no special clinical training requirements and simplified sterilization and maintenance needs. It meshes well with the current workflow of MRI-guided prostate procedures. These attributes make the device cost-effective and accessible to many IR institutions that have already invested in an MRI infrastructure and even to office-based clinics with newly emerging low-field MR systems.[23] The main target applications are MRI-guided prostate procedure which require TP needle placement including a variety of ablation technology applications and biopsies.

2. METHOD

This section explains both the components of this navigation system and how these components work together to fit the clinical workflow.

2.1 Access Tool

The access tool is comprised of four main parts (see Figure 1):

1. the base which slides under the patient and rigidly holds other parts together;
2. the frame and grid which has needle guidance holes and is touching the perineum;
3. the retainer walls which keep the working area clear and the grid accessible;
4. and the optical head which is a stereo camera system.

The design of the grid and the base were based on the grid which is currently being used at Mayo Clinic (Rochester, MN).[24] This grid is not commercially available and lacks features needed for automatic registration and easy access.

In our design, the frame embeds four multi-modality markers called VisiMARKER^{TM}. These markers have a visual pattern (AprilTag[25]) which can be detected and localized by the optical head. They are also visible in MRI and CT volumes. Specifically for MRI volumes, they appear as donuts and are visible in at least the regular T1 and T2 sequences and some other sequences used for prostate imaging.

Figure 2. In addition to the regular straight grid, two angled grids were made.

The frame has a window to access the perineum. Multiple swappable grids may be placed in this window depending on the application. It is also possible to entirely remove the grid for freehand procedures. All the components are designed to be compatible with MRI, CT, and ultrasound imaging.

As shown in Figure 2, a variation of the grid with angled holes allows the physician to avoid obstacles such as rectum or reach the targets which cannot be accessed with the regular straight grid. We 3D-printed the grids with a Stereolithography (SLA) printer (Formlabs, Somerville, MA). For the angled grids, four columns of holes on each side were angled inwards or outwards with a 14-degree slant. The frame and the grid are attached to the base with two posts which can have multiple sizes for better access.

2.2 Planning and navigation software

The software for this tool is based on the Clear Guide SCENERGY platform. Clear Guide SCENERGY is a navigation and guidance system with fusion and tool tracking capabilities. This system is commercially available and is being used for CT/US and MR/US fusion in procedures such as liver biopsy and ablation. We have modified this system to include a planning facility and work with a customized MRI-compatible guidance hardware.

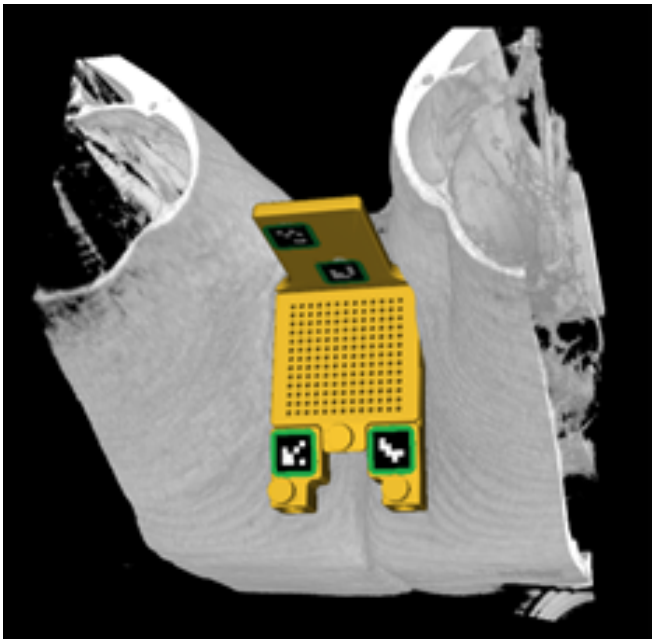

Figure 3. Automatically detected grid within MRI.

The software automatically detects these MRI markers within MRI volumes initially obtained from the patient and locates the grid within the volume (Figure 3).

The optical head is connected to a computational unit and sends a stream of stereo images. The Clear Guide tool tracking module uses the stream of live images to both localize the grid and track ablation or biopsy needles as they appear in the scene. The software also projects the grid holes along the hole directions onto each individual MRI slice. This projected grid is overlaid on top of the 2D slices (Figure 4). In case of freehand insertion, the grid is removed and instead a projection of where the needle will cross the plane is displayed. The physician can browse through the slices and select a target. Once a target is selected, the system highlights the closest hole to that target as shown in Figure 4. The user interface also displays information such as the distance of the target to the grid, the distance of the needle to the target, and the labels of the closest hole. The physician can review the needle path by navigating through the slices.

The projection of the grid depends on the type of the grid that is being used. All the holes can be aligned as in the regular grid (Figure 4a) or multiple columns may be angled inwards or outwards with respect to the medial plane (Figures 4b and 4c).

This software runs on an all-in-one medical computer re-engineered to be used inside the MRI room (outside of the 150 Gauss line). All large ferromagnetic components of this computer have been replaced by non-ferromagnetic material such as aluminum resulting in minimal pull by the magnet event near the bore making it "MR–conditional". This computer is mounted on an MRI compatible cart which is tethered for additional safety.

3. RESULTS

To test this system, we built a phantom with MRI visible targets (Figure 5). The main body phantom was made from gelatin with a preservative while the targets were made from synthetic gel. As shown in Figure 5,

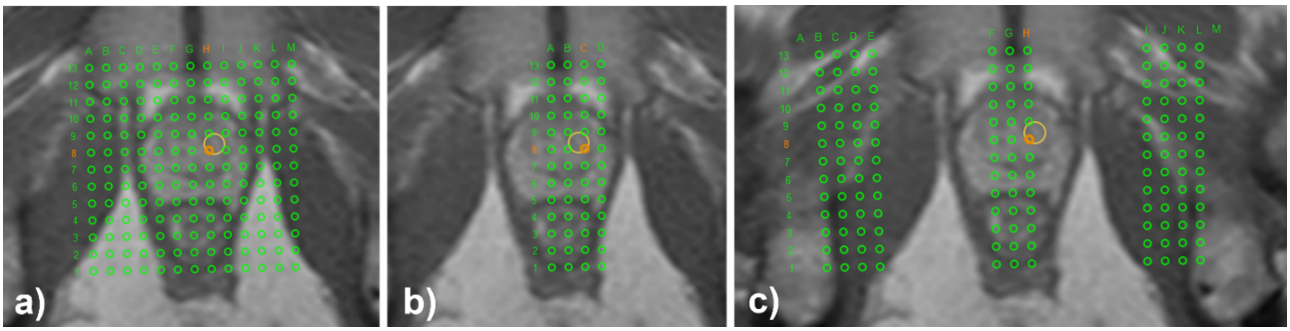

Figure 4. The grid overlay with a selected target; a) regular grid; b) grid with holes angled towards the medial plane; c) grid with holes angled away the medial plane.

the targets appear as dark spheres in this phantom.

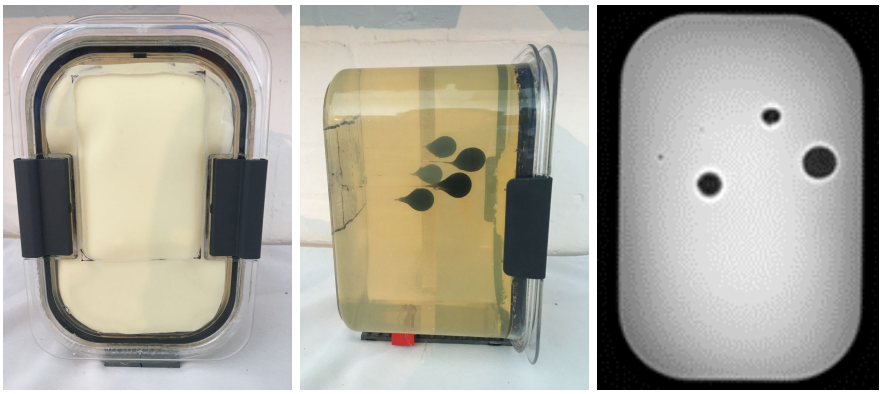
Figure 5. Custom built phantom and its T2 weighted MRI

For the experiment, we fixed the phantom to the base and collected an initial volume. We planned three target points on this volume. These points were selected around the dark spheres and not directly in them since the needle tip cannot be segmented in the dark areas. For each target point, we inserted a needle in the grid hole determined by the software (Figure 6). The needles were the same ones used for prostate biopsies and ablation at Mayo Clinic (BD Angiocath, 14 GA, 5.25 IN). These are MRI compatible introducer needles with a metallic core which is removed during confirmatory imaging leaving only the non-metallic sleeve in the phantom.

Once the three needles were inserted, we collected a post-insertion volume for validation. We repeated this experiment 7 times for a total of 21 insertions. The insertions were divided among the three grid types, straight, outward, and inward as described in Table 1.

Grid Type	Straight	Outward	Inward	overall
Number of Insertions	9	6	6	21
Targeting Error	2.75	2.41	3.08	2.74
STD	1.14	1.49	1.77	1.46
Average Depth	89.2	77.4	85.7	84.9

Table 1. Experiment Results (mm)

To estimate the tip localization error, we manually segmented the needle tip in post-insertion MRIs of the phantom and compared that to the plan. With an average insertion depth of about 85 mm, the average error of needle tip placement was 2.74 mm. Table 1 summarizes the experiment results. The error values for the three types of grids (straight, uutward, and inward angled) are close to each other.

Figure 7 shows two slices of the phantom with three needles inserted. The grid pattern is also projected over these slices. One slice is at the depth of 37 mm (Figure 7 left) and the other one is at 71 mm (Figure 7 right).

Figure 6. Phantom testing

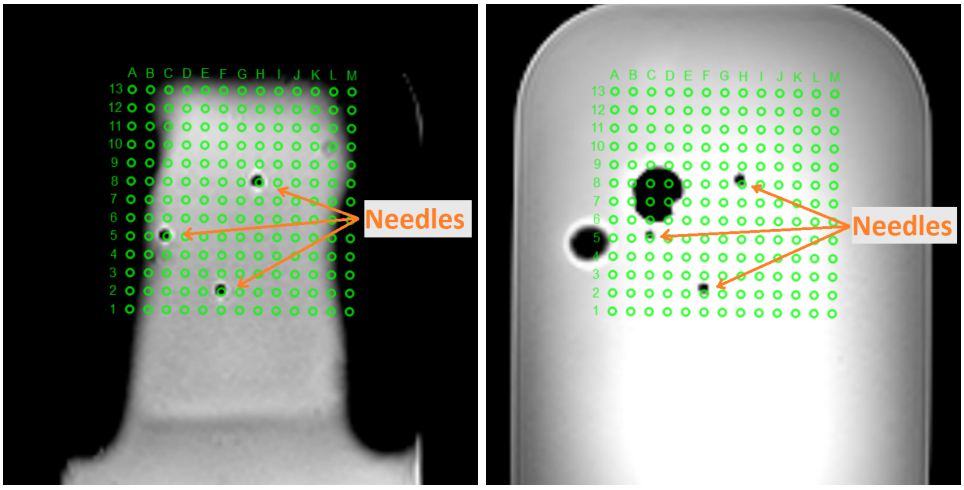

Figure 7. Two slices with grid projection showing the inserted needles at the insertion depths of 37 mm (left) and 71 mm (right).

These figures reveal that the error increases as the needle is inserted deeper as expected. However, the direction of error is not consistent among the three needles suggesting that needle deflection is playing a major role in the increased error.

4. DISCUSSION

We have identified the main sources which contributed to the reported error. The first source seems to be needle deflection. The stiffness of the phantom and the beveled tip of the needles seems to have caused the needles to deflect during insertion (Figure 7). A softer phantom which mimics real tissue more closely and a needle that is not beveled at the tip can reduce this error. We also identified a small mismatch between the expected geometry

from the CAD models and the 3D-printed grids. This problem has been addressed since then by machining the grids instead of printing them. Also, there may have been a small calibration error in volumetric measurements from the MRI machine we used during our experiments (3T Canon). This MRI machine was research-only and may have not been maintained as rigorously as a clinical system.

Other sources of error include the placement of the grid within the frame window, the looseness of grid holes, and human insertion error. For these shortcomings, a frame made with tighter tolerances and a grid with tighter holes as well as freehand insertion with real-time feedback can be helpful.

Another limitation is that the error measurement accuracy is limited by the resolution of the MRI. The obtained MRIs have high axial resolution but the lateral spacing was 2 mm. Identification of needle tip in MRI was also challenging. The needle core which is removed during imaging advances a few millimeters further than the needle shaft which may have affected the error measurements.

5. CONCLUSION

We demonstrated early results of a guidance device for perineal access during MRI-Guided Prostate Interventions such as biopsies and ablations. This device provides a simple and intuitive workflow. It also allows for a more flexible targeting where customized grids can be used to avoid obstacles. The grids may be swapped mid-procedure if required by the procedure. The other advantage is that the guidance feedback and more accurate needle placement will likely reduce the number of intermediary images required for needle adjustments resulting in a reduction of the overall procedure time. We are conducting a clinical trial with an updated version of this system. Future work also includes freehand guidance with live needle tracking as well as ultrasound and MR fusion.

REFERENCES

[1] Society, A. C., "Cancer Facts and Figures, 2022." www.cancer.org/cancer/prostate-cancer/about/key-statistics.html (2022). [Online; accessed Sept 3, 2022].

[2] Serefoglu, E. C., Altinova, S., Ugras, N. S., Akincioglu, E., Asil, E., and Balbay, D., "How reliable is 12-core prostate biopsy procedure in the detection of prostate cancer?," *Canadian Urological Association Journal* **7**(5-6), e293–8 (2013).

[3] Borghesi, M., Ahmed, H., Nam, R., Schaeffer, E., Schiavina, R., Taneja, S., Weidner, W., and Loeb, S., "Complications after systematic, random, and image-guided prostate biopsy," *European urology* **71**(3), 353–365 (2017).

[4] Meyer, A. R., Mamawala, M., Winoker, J. S., Landis, P., Epstein, J. I., Macura, K. J., Allaf, M. E., Partin, A. W., Pavlovich, C. P., and Gorin, M. A., "Transperineal prostate biopsy improves the detection of clinically significant prostate cancer among men on active surveillance," *The Journal of urology* **205**(4), 1069–1074 (2021).

[5] Liss, M. A., Ehdaie, B., Loeb, S., Meng, M. V., Raman, J. D., Spears, V., and Stroup, S. P., "An update of the american urological association white paper on the prevention and treatment of the more common complications related to prostate biopsy," *The Journal of urology* **198**(2), 329–334 (2017).

[6] Loeb, S., Vellekoop, A., Ahmed, H. U., Catto, J., Emberton, M., Nam, R., Rosario, D. J., Scattoni, V., and Lotan, Y., "Systematic review of complications of prostate biopsy," *European urology* **64**(6), 876–892 (2013).

[7] Gross, M. D., Alshak, M. N., Shoag, J. E., Laviana, A. A., Gorin, M. A., Sedrakyan, A., and Hu, J. C., "Healthcare costs of post-prostate biopsy sepsis," *Urology* **133**, 11–15 (2019).

[8] Evans, R., Loeb, A., Kaye, K. S., Cher, M. L., and Martin, E. T., "Infection-related hospital admissions after prostate biopsy in united states men," in [*Open forum infectious diseases*], **4**(1), ofw265, Oxford University Press US (2017).

[9] Bass, E., Donaldson, I., Freeman, A., Jameson, C., Punwani, S., Moore, C., Arya, M., Emberton, M., and Ahmed, H., "Magnetic resonance imaging targeted transperineal prostate biopsy: a local anaesthetic approach," *Prostate cancer and prostatic diseases* **20**(3), 311–317 (2017).

[10] Bhatt, N. R., Breen, K., Haroon, U. M., Akram, M., Flood, H. D., and Giri, S. K., "Patient experience after transperineal template prostate biopsy compared to prior transrectal ultrasound guided prostate biopsy," *Central European Journal of Urology* **71**(1), 43 (2018).

[11] Xiang, J., Yan, H., Li, J., Wang, X., Chen, H., and Zheng, X., "Transperineal versus transrectal prostate biopsy in the diagnosis of prostate cancer: a systematic review and meta-analysis," *World journal of surgical oncology* **17**(1), 1–11 (2019).

[12] Pilatz, A., Veeratterapillay, R., Dimitropoulos, K., Omar, M. I., Pradere, B., Yuan, Y., Cai, T., Mezei, T., Devlies, W., Bruyere, F., et al., "European association of urology position paper on the prevention of infectious complications following prostate biopsy," *European urology* **79**(1), 11–15 (2021).

[13] Pokorny, M. R., De Rooij, M., Duncan, E., Schröder, F. H., Parkinson, R., Barentsz, J. O., and Thompson, L. C., "Prospective study of diagnostic accuracy comparing prostate cancer detection by transrectal ultrasound–guided biopsy versus magnetic resonance (mr) imaging with subsequent mr-guided biopsy in men without previous prostate biopsies," *European urology* **66**(1), 22–29 (2014).

[14] Woodrum, D. A., Kawashima, A., Gorny, K. R., and Mynderse, L. A., "Targeted prostate biopsy and mr-guided therapy for prostate cancer," *Abdominal Radiology* **41**(5), 877–888 (2016).

[15] Kyle, K. Y. and Hricak, H., "Imaging prostate cancer," *Radiologic Clinics of North America* **38**(1), 59–85 (2000).

[16] Sherman, A., Kuftinec, D., Price, L. L., Moinzadeh, A., and Faust, W., "Mp58-19 comparison of uronav trus and cognitive fusion tp biopsy in detection of clinically significant prostate cancer," *The Journal of Urology* **207**(Supplement 5), e999 (2022).

[17] Krieger, A., Iordachita, I. I., Guion, P., Singh, A. K., Kaushal, A., Ménard, C., Pinto, P. A., Camphausen, K., Fichtinger, G., and Whitcomb, L. L., "An mri-compatible robotic system with hybrid tracking for mri-guided prostate intervention," *IEEE Transactions on Biomedical Engineering* **58**(11), 3049–3060 (2011).

[18] Fisher, T., Hamed, A., Vartholomeos, P., Masamune, K., Tang, G., Ren, H., and Tse, Z. T., "Intraoperative magnetic resonance imaging–conditional robotic devices for therapy and diagnosis," *Proceedings of the Institution of Mechanical Engineers, Part H: Journal of Engineering in Medicine* **228**(3), 303–318 (2014).

[19] Muntener, M., Patriciu, A., Petrisor, D., Schar, M., Ursu, D., Song, D. Y., and Stoianovici, D., "Transperineal prostate intervention: robot for fully automated mr imaging—system description and proof of principle in a canine model," *Radiology* **247**(2), 543–549 (2008).

[20] Stoianovici, D., Jun, C., Lim, S., Li, P., Petrisor, D., Fricke, S., Sharma, K., and Cleary, K., "Multi-imager compatible, mr safe, remote center of motion needle-guide robot," *IEEE Transactions on Biomedical Engineering* **65**(1), 165–177 (2017).

[21] Fütterer, J. J. and Barentsz, J. O., "Mri-guided and robotic-assisted prostate biopsy," *Current opinion in urology* **22**(4), 316–319 (2012).

[22] Patel, N. A., Azimi, E., Monfaredi, R., Sharma, K., Cleary, K., and Iordachita, I., "Robotic system for mri-guided shoulder arthrography: Accuracy evaluation," in [*2018 International Symposium on Medical Robotics (ISMR)*], 1–6, IEEE (2018).

[23] Chiragzada, S., Hellman, E., Michael, D., Narayanan, R., Nacev, A., and Kumar, D., "Initial phantom studies for an office-based low-field mr system for prostate biopsy," *International Journal of Computer Assisted Radiology and Surgery* **16**(5), 741–748 (2021).

[24] Woodrum, D. A., Gorny, K. R., Greenwood, B., and Mynderse, L. A., "Mri-guided prostate biopsy of native and recurrent prostate cancer," in [*Seminars in Interventional Radiology*], **33**(03), 196–205, Thieme Medical Publishers (2016).

[25] Olson, E., "Apriltag: A robust and flexible visual fiducial system," in [*2011 IEEE international conference on robotics and automation*], 3400–3407, IEEE (2011).